Structural Engineering and Mechanics, *Vol. 53, No. 6 (2015) 1167-1182*
DOI: http://dx.doi.org/10.12989/sem.2015.53.6.1167

Electric potential redistribution due to time-dependent creep in thick-walled FGPM cylinder based on Mendelson method of successive approximation

S. Kheirkhah*[1] and A. Loghman[2]

[1]*Department of Mechanical Engineering, Kashan Branch, Islamic Azad University, Kashan, Iran*
[2]*Faculty of Mechanical Engineering, University of Kashan, Kashan, Iran*

(Received August 7, 2014, Revised October 6, 2014, Accepted October 29, 2014)

Abstract. In this study, the stresses and electric potential redistributions of a cylinder made from functionally graded piezoelectric material (FGPM) are investigated. All the mechanical, thermal and piezoelectric properties are modeled as power-law distribution of volume fraction. Using the coupled electro-thermo-mechanical relations, strain-displacement relations, Maxwell and equilibrium equations are obtained including the time dependent creep strains. Creep strains are time, temperature and stress dependent, the closed form solution cannot be found for this constitutive differential equation. A semi-analytical method in conjunction with the Mendelson method of successive approximation is therefore proposed for this analysis. Similar to the radial stress histories, electric potentials increase with time, because the latter is induced by the former during creep deformation of the cylinder, justifying industrial application of such a material as efficient actuators and sensors.

Keywords: mendelson method of successive approximation; time-dependent creep; cylinder; FGPM

1. Introduction

Piezoelectric effect has important uses in modern engineering because it expresses the connection between the electrical and mechanical fields which has wide applications in electro-mechanical devices, such as actuators, sensors and transducers. Recently, a new class of composite materials known as functionally graded materials (FGMs) has drawn considerable attention. A typical FGM, with a high bending–stretching coupling effect, is an inhomogeneous composite made from different phases of material constituents (usually ceramic and metal).

The first idea for producing FGMs was their application in high temperature environment and improving their mechanical properties. These materials which are mainly constructed to operate in high temperature environments, find their application in nuclear reactors, chemical laboratories, aerospace, turbine rotors, flywheels and pressure vessels. As the use of FGMs increases, new methodologies need to be developed to characterize, analyze and design structural components made of these materials.

Thermoelectroelastic analysis of FGPM components has been investigated by many

*Corresponding author, Ph.D., E-mail: dr.saeedkherikhah@gmail.com

http://www.techno-press.org/?journal=sem&subpage=8 ISSN: 1225-4568 (Print), 1598-6217 (Online)

researchers. Mechanical and thermal stresses in a functionally graded hollow cylinder due to radially symmetric were investigated by Jabbari *et al*. (2002). Analysis of the thermal stress behavior of functionally graded hollow circular cylinders was presented by Liew *et al*. (2003). You (2005) presented elastic analysis of internally pressurized thick-walled spherical pressure vessels of functionally graded materials. Dai *et al*. (2006) studied exact solutions for functionally graded pressure vessels in a uniform magnetic field. Coupled thermoelasticity of functionally graded cylindrical shells was developed by Bahtui and Eslami (2007). Recently Ghorbanpour Arani *et al*. (2011a) investigated the effect of material in-homogeneity on electro-thermo-mechanical behaviors of functionally graded piezoelectric rotating shaft. Also, they (2011b) were studied electro-thermo-mechanical behaviors of FGPM spheres using analytical method and ANSYS software.

None of the above studies have considered creep deformation of the FGPM cylinders. Pai (1967) investigated steady-state creep analysis of thick-walled orthotropic cylinders. Sim and Penny (1971) analyzed plane strain creep behavior of thick-walled cylinders. Bhatnagar and Arya (1974) investigated large strain creep deformation of a thick-walled cylinder of an anisotropic material subjected to internal pressure. Simonian (1979) calculated the thermal stresses in thick-walled cylinders taking account of non-linear creep. Yang (2000) presented a solution for time-dependent creep behavior of FGM cylinders using Norton's law for material creep constitutive model. Steady-state creep of a pressurized thick cylinder in both the linear and the power law ranges was investigated by Altenbach *et al*. (2008). Loghman *et al*. (2010) studied the Magnetothermoelastic creep analysis of functionally graded cylinders. They found that radial stress redistributions are not significant for different material properties, however major redistributions occur for circumferential and effective stresses. Semi-analytical solution of time-dependent electro-thermo-mechanical creep for radially polarized piezoelectric cylinder was investigated by Ghorbanpour Arani *et al*. (2011). They found that Similar to the radial stress histories, electric potentials increase with time. Using method of successive elastic solution, Loghman *et al*. (2012) studied magnetothermoelastic creep behavior of thick-walled FGM spheres placed in uniform magnetic and distributed temperature fields and subjected to an internal pressure. They showed that stresses, strains and effective creep strain rate are changing in time with a decreasing rate so that after almost 50 years the time-dependent solution approaches the steady state condition when there is no distinction between stresses and strains at 50 and 55 years. Recently, time-dependent behaviors of a FGPM hollow sphere under the coupling of multi-fields were presented by Dai *et al*. (2012). They assumed that material properties, electric parameters, permeability, thermal conductivity and creep parameters vary smoothly through the radial direction of the FGPM spherical structure according to a simple power-law.

Apart from a couple of studies, prepared by a few authors here, little or no reference has been made so far in the literature on the time-dependent creep analysis of FGPM cylinders. It has been shown by Zhou and kamlah (2006) that even at room temperature ferroelectric piezoceramics exhibit significant creep effects. This creep is of a primary type and can be expressed by a power law constitutive model. To improve the performance and reliability of piezoactuators used for high-precision applications, time-dependent creep analysis must be considered when these devices are used even at room temperatures.

However, to date, no report has been found in the literature on the time dependent creep behavior of hollow FGPM cylinders based on power-law distribution of mechanical, thermal and piezoelectric properties. Motivated by these considerations, we aim to investigate history of stresses, strains, deformation and electric potential of a thick hollow FGPM cylinder made of

radially polarized anisotropic piezoelectric material using a semi-analytical method base on Mendelson's method of successive elastic solution.

2. Heat conduction problem

In this study a distributed temperature field due to steady-state heat conduction has been considered. The steady-state, heat transfer equation in the FGPM cylinder with inner radius *a* and outer radius *b* is solved with the assumed boundary conditions (Ghorbanpour Arani *et al*. 2011a)

$$\frac{1}{r}\frac{d}{dr}\left(k(r)r\frac{d}{dr}T\left(r\right)\right)=0, \tag{1}$$

$$\begin{aligned} T(a)&=T_a,\\ T(b)&=T_b, \end{aligned} \tag{2}$$

where (′) denotes differentiation with respect to *r*, $K=K(r)$ is the thermal conductivity and A_{ij}, $i,j=(1,2)$ and either designate the thermal conductivity or the heat transfer coefficient depending on the type of thermal boundary conditions employed. The constants f_1 and f_2 have known values on the inner and outer radius, respectively. It is assumed that the non-homogeneous thermal conductivity $K(r)$ is a power function of the radius

$$K(r)=K_0r^{\gamma}, \tag{3}$$

where γ is in-homogeneity material parameter. Using Eq. (3) into Eq. (1) for the thermal conductivity, the heat conduction equation can be written as

$$\frac{1}{r}\frac{d}{dr}\left(K_0r^{\gamma+1}\frac{d}{dr}T\left(r\right)\right)=0. \tag{4}$$

Integrating Eq. (4) yields

$$T(r)=-\frac{F_1}{\gamma}r^{-\gamma}+F_2. \tag{5}$$

Applying the boundary conditions (2) results in the following relations for the coefficients A_1 and A_2

$$A_1=\frac{\left(T_a-T_b\right)\left(\frac{b}{a}\right)^{\beta}}{1-\left(\frac{b}{a}\right)^{\beta}}, \tag{6}$$

$$A_2=\frac{\left(T_b-T_a\right)b^{\beta}}{1-\left(\frac{b}{a}\right)^{\beta}}. \tag{7}$$

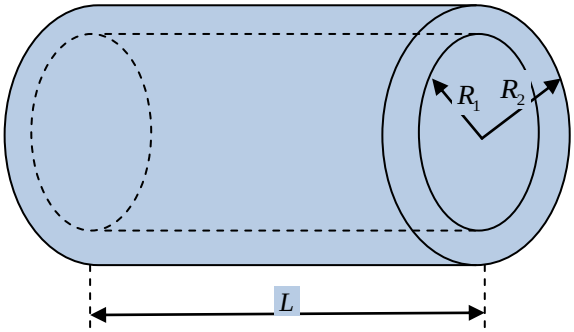

Fig. 1 Hollow FGPM circular cylinder subject to uniform temperature field, uniform internal pressure, uniform external pressure and applied voltage V

3. Basic formulation of hollow FGPM cylinder

A hollow FGPM cylinder with inner and outer radius of a and b subjected to an inner pressure, thermal gradient and an electric potential is considered (Fig. 1).

The components of displacement and electric potential are assumed

$$\begin{aligned} u_r &= u(r), \\ u_z &= 0, \\ u_\theta &= 0, \\ \phi &= \phi(r). \end{aligned} \tag{8}$$

The equation of equilibrium considering the inertia body force and the Maxwell's equation for free electric charge density are written as (Ghorbanpour Arani *et al*. 2011a, 2011b)

$$\frac{\partial \sigma_{rr}}{\partial r} + \frac{\sigma_{rr} - \sigma_{\theta\theta}}{r} = 0, \tag{9}$$

$$\frac{\partial D_{rr}}{\partial r} + \frac{D_{rr}}{r} = 0, \tag{10}$$

where $\sigma_{ii}(i=r,\theta)$ and D_{rr} are the stress tensor and electric displacement, respectively.

Also, the strain-displacement and the relation between electric field and electric potential are reduced as

$$\varepsilon_{rr} = \frac{\partial u}{\partial r}, \tag{11}$$

$$\varepsilon_{\theta\theta} = \frac{u}{r}, \tag{12}$$

$$E_{rr} = -\frac{\partial \phi}{\partial r}. \tag{13}$$

The constitutive relations of cylindrically orthotropic radially polarized piezoelectric media and the component of radial electric displacement vector also can be written as (Ghorbanpour Arani *et al*. 2011, Tiersten 1969)

$$\sigma_{rr} = C_{11}\left(\varepsilon_{rr} - \varepsilon_{rr}^{c} - \alpha_{rr}T(r)\right) + C_{12}\left(\varepsilon_{\theta\theta} - \varepsilon_{\theta\theta}^{c} - \alpha_{\theta\theta}T(r)\right) - e_{11}E_{rr}, \tag{14}$$

$$\sigma_{\theta\theta} = C_{12}\left(\varepsilon_{rr} - \varepsilon_{rr}^{c} - \alpha_{rr}T(r)\right) + C_{22}\left(\varepsilon_{\theta\theta} - \varepsilon_{\theta\theta}^{c} - \alpha_{\theta\theta}T(r)\right) - e_{12}E_{rr}, \tag{15}$$

$$\sigma_{\theta\theta} = C_{12}\left(\varepsilon_{rr} - \varepsilon_{rr}^{c} - \alpha_{rr}T(r)\right) + C_{22}\left(\varepsilon_{\theta\theta} - \varepsilon_{\theta\theta}^{c} - \alpha_{\theta\theta}T(r)\right) - e_{12}E_{rr}, \tag{16}$$

where c_{ij} (i,j=1,2), e_{1j} (i=1,2), α_i (i=r,θ) and $\in_{11}$ are elastic constants, piezoelectric constants, thermal expansion coefficients, dielectric constants, respectively.

For the analysis, the following dimensionless quantities are introduced as

$$\begin{aligned}
&\Sigma_r = \frac{\sigma_{rr}}{C_{22}^{0}}, \qquad \Sigma_\theta = \frac{\sigma_{\theta\theta}}{C_{22}^{0}}, \quad U = \frac{u}{R_1}, \quad \chi = \frac{r}{R_i}, \qquad \beta = \frac{R_0}{R_i},\\
&\Phi = \frac{\phi}{\phi_0}, \qquad \phi_0 = R_i\sqrt{\frac{C_{22}^{0}}{\in_{11}}}, \quad \Psi_r = \frac{D_{rr}}{\sqrt{C_{22}^{0}\in_{11}}}, \qquad C_1 = \frac{C_{11}^{0}}{C_{22}^{0}},\\
&C_2 = \frac{C_{12}^{0}}{C_{22}^{0}}, \qquad \Xi_1 = \frac{e_{11}}{\sqrt{C_{22}^{0}\in_{11}}}, \qquad \Xi_2 = \frac{e_{12}}{\sqrt{C_{22}^{0}\in_{11}}}.
\end{aligned} \tag{17}$$

Using the above dimensionless variables, Eqs. (5), (9)-(10) can be expressed as

$$T(\chi) = -\frac{F_1}{\gamma}\chi^{-\gamma} + F_2, \tag{18}$$

$$\frac{\partial\Sigma_r}{\partial\chi} + \frac{\Sigma_r - \Sigma_\theta}{\chi} = 0, \tag{19}$$

$$\frac{\partial\Psi_r}{\partial\chi} + \frac{\Psi_r}{\chi} = 0. \tag{20}$$

Before substituting the component of the electric field in Maxwell's equation, appropriate functions for all properties are assumed as

$$\Psi_r = \Psi_0\left(\frac{r}{a}\right)^{\gamma}, \tag{21}$$

in which Ψ_r represents the general properties of the cylinder such as the elastic, piezoelectric, and dielectric coefficients, and Ψ_0 corresponds to the value of the coefficients at the outer surface. Substituting Eqs. (17) and (21) into Eqs. (14)-(16) the two components of the stresses and the radial electric displacement are obtained as

$$\Sigma_r = C_1\chi^{\gamma}\left(\frac{dU}{d\chi} - \varepsilon_{rr}^{c} - \alpha_{rr}^{0}\chi^{\gamma}\left(-\frac{F_1}{\gamma}\chi^{-\gamma} + F_2\right)\right) + C_2\chi^{\gamma}\left(\frac{U}{\chi} - \varepsilon_{\theta\theta}^{c} - \alpha_{\theta\theta}^{0}\chi^{\gamma}\left(-\frac{F_1}{\gamma}\chi^{-\gamma} + F_2\right)\right) + \Xi_1\chi^{\gamma}\frac{d\Phi}{d\chi}, \tag{22}$$

$$\Sigma_\theta = C_2\chi^\gamma\left(\frac{dU}{d\chi}-\varepsilon^c_{rr}-\alpha^0_{rr}\chi^\gamma\left(-\frac{F_1}{\gamma}\chi^{-\gamma}+F_2\right)\right)+\chi^\gamma\left(\frac{U}{\chi}-\varepsilon^c_{\theta\theta}-\alpha^0_{\theta\theta}\chi^\gamma\left(-\frac{F_1}{\gamma}\chi^{-\gamma}+F_2\right)\right)+\Xi_2\chi^\gamma\frac{d\Phi}{d\chi}, \tag{23}$$

$$\Psi_r = \Xi_1\chi^\gamma\left(\frac{dU}{d\chi}-\varepsilon^c_{rr}-\alpha^0_{rr}\chi^\gamma\left(-\frac{F_1}{\gamma}\chi^{-\gamma}+F_2\right)\right)+\Xi_2\chi^\gamma\left(\frac{U}{\chi}-\varepsilon^c_{\theta\theta}-\alpha^0_{\theta\theta}\chi^\gamma\left(-\frac{F_1}{\gamma}\chi^{-\gamma}+F_2\right)\right)-\chi^\gamma\frac{d\Phi}{d\chi}. \tag{24}$$

4. Solution procedure

The solution of Eq. (20) is

$$\Psi_r = \frac{F_3}{\chi}, \tag{25}$$

where F_1 is a constant. Substituting Eq. (25) into Eq. (16), we obtain

$$\begin{aligned}\frac{d\Phi}{d\chi} = &-F_3\chi^{-\gamma-1}+\Xi_1\left(\frac{dU}{d\chi}-\varepsilon^c_{rr}-\alpha^0_{rr}\chi^\gamma\left(-\frac{F_1}{\gamma}\chi^{-\gamma}+F_2\right)\right)\\ &+\Xi_2\left(\frac{U}{\chi}-\varepsilon^c_{\theta\theta}-\alpha^0_{\theta\theta}\chi^\gamma\left(-\frac{F_1}{\gamma}\chi^{-\gamma}+F_2\right)\right).\end{aligned} \tag{26}$$

Substituting Eq. (26) into Eqs. (14) and (15), leads to

$$\begin{aligned}\Sigma_r = &L_1\chi^\gamma\left(\frac{dU}{d\chi}-\varepsilon^c_{rr}-\alpha^0_{rr}\chi^\gamma\left(-\frac{F_1}{\gamma}\chi^{-\gamma}+F_2\right)\right)\\ &+L_2\chi^\gamma\left(\frac{U}{\chi}-\varepsilon^c_{\theta\theta}-\alpha^0_{\theta\theta}\chi^\gamma\left(-\frac{F_1}{\gamma}\chi^{-\gamma}+F_2\right)\right)-F_3\Xi_1\chi^{-1},\end{aligned} \tag{27}$$

$$\begin{aligned}\Sigma_\theta = &L_2\chi^\gamma\left(\frac{dU}{d\chi}-\varepsilon^c_{rr}-\alpha^0_{rr}\chi^\gamma\left(-\frac{F_1}{\gamma}\chi^{-\gamma}+F_2\right)\right)\\ &+L_3\chi^\gamma\left(\frac{U}{\chi}-\varepsilon^c_{\theta\theta}-\alpha^0_{\theta\theta}\chi^\gamma\left(-\frac{F_1}{\gamma}\chi^{-\gamma}+F_2\right)\right)-F_3\Xi_2\chi^{-1},\end{aligned} \tag{28}$$

where

$$L_1 = C_1+\Xi_1^2, \qquad L_2 = C_2+\Xi_1\Xi_2, \quad L_3 = 1+\Xi_2^2. \tag{29}$$

Electric potential ϕ is obtained by integrating the Eq. (26)

$$\Phi = \int\left(\begin{aligned}&-F_3\chi^{-\gamma-1}+\Xi_1\left(\frac{dU}{d\chi}-\varepsilon^c_{rr}-\alpha^0_{rr}\chi^\gamma\left(-\frac{F_1}{\gamma}\chi^{-\gamma}+F_2\right)\right)\\ &+\Xi_2\left(\frac{U}{\chi}-\varepsilon^c_{\theta\theta}-\alpha^0_{\theta\theta}\chi^\gamma\left(-\frac{F_1}{\gamma}\chi^{-\gamma}+F_2\right)\right)\end{aligned}\right)d\chi. \tag{30}$$

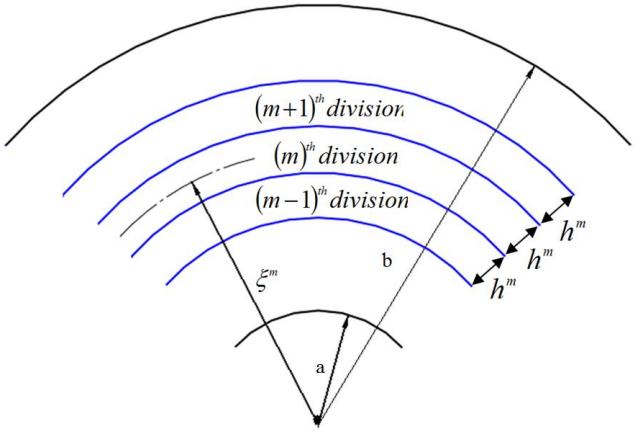

Fig. 2 Dividing radial domain into some finite sub-domains

Finally, substituting Eqs. (27) and (28) into Eq. (19) yields the following in-homogeneous ordinary differential equation containing time-dependent creep strains

$$\begin{aligned}\chi^2\frac{d^2U}{d\chi^2}+\chi L_1\frac{dU}{d\chi}+L_2U &= -F_1L_3\chi-F_2L_4\chi^{1+\gamma}\\ -F_3L_5\chi^{-\gamma}-L_6\chi\varepsilon_{rr}^c-L_7\chi\varepsilon_{\theta\theta}^c+\chi^2\frac{\partial\varepsilon_{rr}^c}{\partial\chi}&+L_8\chi^2\frac{\partial\varepsilon_{\theta\theta}^c}{\partial\chi},\end{aligned} \tag{31}$$

where

$$L_1=(1+\gamma),\quad L_2=\frac{\gamma\left(C_2+\Xi_1\Xi_2\right)-\left(1+\Xi_2^2\right)}{\left(C_1+\Xi_1^2\right)},$$

$$L_3=\frac{\left[\left(\gamma+1\right)\left(C_1+\Xi_1^2\right)-\left(C_2+\Xi_1\Xi_2\right)\right]\alpha_{rr}^0+\left[\left(\gamma+1\right)\left(C_2+\Xi_1\Xi_2\right)-\left(1+\Xi_2^2\right)\right]\alpha_{\theta\theta}^0}{\left(C_1+\Xi_1^2\right)},$$

$$L_4=\frac{\left[\left(-2\gamma-1\right)\left(C_1+\Xi_1^2\right)+\left(C_2+\Xi_1\Xi_2\right)\right]\alpha_{rr}^0+\left[\left(-2\gamma-1\right)\left(C_2+\Xi_1\Xi_2\right)+\left(1+\Xi_2^2\right)\right]\alpha_{\theta\theta}^0}{\left(C_1+\Xi_1^2\right)}, \tag{32}$$

$$L_5=\frac{\Xi_2}{\left(C_1+\Xi_1^2\right)},\qquad L_6=\frac{\left(-\gamma-1\right)\left(C_1+\Xi_1^2\right)+\left(C_2+\Xi_1\Xi_2\right)}{\left(C_1+\Xi_1^2\right)},$$

$$L_7=\frac{\left(-\gamma-1\right)\left(C_2+\Xi_1\Xi_2\right)+\left(1+\Xi_2^2\right)}{\left(C_1+\Xi_1^2\right)},\qquad L_8=\frac{-\left(C_2+\Xi_1\Xi_2\right)}{\left(C_1+\Xi_1^2\right)}.$$

Eq. (31) is a non-homogeneous second-order ordinary differential equation containing time-dependent creep strains for displacement field in the FGPM hollow rotating cylinder.

4.1 Semi-analytical solution for thermo-electro- elastic analysis of rotating cylinder

A semi-analytical method for solution of the differential Eq. (31) has been applied. The solution domain is first divided into some finite divisions as shown in Fig. 2.

The coefficients of Eq. (31) are evaluated at ξ^m, mean radius of m^{th} division, and therefore, the differential equation with constant coefficients become valid only for the m^{th} sub-domain which can be re-written as (Kordkheili *et al*. 2007, Bayat *et al*. 2009)

$$\left(K_1^{\,m}\frac{d^2}{d\chi^2}+K_2^{\,m}\frac{d}{d\chi}+K_3^{\,m}\right)U^m+K_4^{\,m}=0, \tag{33}$$

$$K_1^m=(\chi^m)^2,$$

$$K_2^m=(1+\gamma)\chi^m,$$

$$K_3^m=\gamma\left(\frac{(C_2+\Xi_1\Xi_2)-(1+\Xi_2^2)}{(C_1+\Xi_1^2)}\right)^m,$$

$$K_4^m=\left[\frac{\left[(\gamma+1)(C_1+\Xi_1^2)-(C_2+\Xi_1\Xi_2)\right]\alpha_{rr}^0+\left[(\gamma+1)(C_2+\Xi_1\Xi_2)-(1+\Xi_2^2)\right]\alpha_{\theta\theta}^0}{(C_1+\Xi_1^2)}\right]^m F_1\chi^m+ \tag{34}$$

(35)

$$\left[\frac{\left[(-2\gamma-1)(C_1+\Xi_1^2)+(C_2+\Xi_1\Xi_2)\right]\alpha_{rr}^0+\left[(-2\gamma-1)(C_2+\Xi_1\Xi_2)+(1+\Xi_2^2)\right]\alpha_{\theta\theta}^0}{(C_1+\Xi_1^2)}\right]^m F_2(\chi^m)^{(1+\gamma)}+ \tag{36}$$

$$\left[\frac{\Xi_2}{(C_1+\Xi_1^2)}\right]^m F_3(\chi^m)^{(-\gamma)}+\left[\frac{-(\gamma-1)(C_1+\Xi_1^2)+(C_2+\Xi_1\Xi_2)}{(C_1+\Xi_1^2)}\right]^m(\chi^m)^3 \tag{37}$$

$$+\left(\left[\frac{(-\gamma-1)(C_1+\Xi_1^2)+(C_2+\Xi_1\Xi_2)}{(C_1+\Xi_1^2)}\right]^m\varepsilon_r^c\Big|_{\chi=\chi^m}+\left[\frac{(-\gamma-1)(C_2+\Xi_1\Xi_2)+(1+\Xi_2^2)}{(C_1+\Xi_1^2)}\right]^m\varepsilon_\theta^c\Big|_{\chi=\chi^m}\right)\chi^m$$

$$+\left(-\frac{\partial\varepsilon_r^c}{\partial\chi}\Big|_{\chi=\chi^m}+\left[\frac{-(C_2+\Xi_1\Xi_2)}{(C_1+\Xi_1^2)}\right]^m\frac{\partial\varepsilon_\theta^c}{\partial\chi}\Big|_{\chi=\chi^m}\right)(\chi^m)^2.$$

Hence, the differential equation can now be solved since the terms corresponding to the creep strain functions on the R.H.S have become known. The general solution for Eq. (33) could be written as follows

$$U_g^m=F_4^{\,m}e^{N_1^{\,m}\chi}+F_5^{\,m}e^{N_2^{\,m}\chi}, \tag{38}$$

where

$$N_1^{\,m},N_2^{\,m}=\frac{-K_2^{\,m}\pm\sqrt{(K_2^{\,m})^2-4K_3^{\,m}K_1^{\,m}}}{2K_1^{\,m}}. \tag{39}$$

The particular solution of the differential Eq. (33) may be written as

$$U_p = X_1. \tag{40}$$

Substituting Eq. (40) into Eq. (33) yields

$$X_1 = \frac{K_4^m}{K_3^m}. \tag{41}$$

The complete solution for U^m in terms of the non-dimensional radial coordinate is therefore written as

$$\chi^m - \frac{h^m}{2} \le \chi \le \chi^m + \frac{h^m}{2}\ U = U_g^m + U_p^m = F_4{}^m e^{N_1{}^m \chi} + F_5{}^m e^{N_2{}^m \chi} + \frac{K_4^m}{K_3^m}, \tag{42}$$

where h^m is the thickness of m^{th} division. Substituting the displacement from Eq. (42) into Eqs. (27)-(28) and (30) the radial and circumferential stresses and electric potential are evaluated.

The unknowns $F_1^m, F_2{}^m, F_3^m, F_4{}^m, F_5{}^m$ and $F_6{}^m$ (the constant of integrating of Eq. (30)) are determined by applying the necessary boundary conditions between two adjacent sub-domains. For this purpose, the continuity of radial displacement, radial stress, temperature and electric potential are imposed at the interfaces of the adjacent sub-domains. These continuity conditions at the interfaces are

$$\begin{aligned}
&U^m\Big|_{\chi=\chi^m+\frac{h^m}{2}} = U^{m+1}\Big|_{\chi=\chi^{m+1}-\frac{h^{m+1}}{2}},\\
&\left.\frac{dU^m}{d\chi}\right|_{\chi=\chi^m+\frac{h^m}{2}} = \left.\frac{dU^{m+1}}{d\chi}\right|_{\chi=\chi^{m+1}-\frac{h^{m+1}}{2}},\\
&\Sigma_r{}^m\Big|_{\chi=\chi^m+\frac{h^m}{2}} = \Sigma_r{}^{m+1}\Big|_{\chi=\chi^{m+1}-\frac{h^{m+1}}{2}},\\
&\Phi^m\Big|_{\chi=\chi^m+\frac{h^m}{2}} = \Phi^{m+1}\Big|_{\chi=\chi^{m+1}-\frac{h^{m+1}}{2}},\\
&T_\chi^m\Big|_{\chi=\chi^m+\frac{h^m}{2}} = T_\chi^m\Big|_{\chi=\chi^{m+1}-\frac{h^{m+1}}{2}},\\
&\left.\frac{\partial T_\chi^m}{\partial\chi}\right|_{\chi=\chi^m+\frac{h^m}{2}} = \left.\frac{\partial T_\chi^m}{\partial\chi}\right|_{\chi=\chi^{m+1}-\frac{h^{m+1}}{2}},
\end{aligned} \tag{43}$$

and global boundary conditions are written in dimensionless form as

$$\Phi(1)=0,\ \ \Phi(\chi)=0, \text{ (Mechanical boundary condition) } \ \Sigma_r(\chi)=0,\ \ \Sigma_r(1)=-1 \tag{44}$$

$$\Sigma_r(\chi)=0,\ \ \Phi(1)=1,\ \ \Phi(\chi)=0. \text{ (electrical boundary condition) } \ \Sigma_r(1)=0 \tag{45}$$

The continuity conditions Eq. (43) together with the global boundary conditions Eqs. (44)-(45) yield a set of linear algebraic equations in terms of $F_1^m, F_2{}^m, F_3^m, F_4{}^m, F_5{}^m$ and $F_6{}^m$. Solving the resultant linear algebraic equations the unknown coefficients are calculated. Then the displacement

component, the stresses and the electric potential are determined in each radial sub-domain. Increasing the number of divisions improves the accuracy of the results.

4.2 Time-dependent thermo-electro- elastic creep behavior of cylinder

To obtain time-dependent stresses and electric potential, the creep strains in Eqs. (27)- (28) and (30) must be considered. Creep strain rates are related to the material creep constitutive model and the current stress tensor by the well known prandtl–Reuss relation. In this case Prandtl-Reuss relation is written as (Penny and Marriott 1995)

$$\dot{\varepsilon}_r = \frac{\dot{\varepsilon}_e}{\Sigma_e}\left[\Sigma_r - 0.5\left(\Sigma_\theta + \Sigma_z\right)\right], \tag{46}$$

$$\dot{\varepsilon}_\theta = \frac{\dot{\varepsilon}_e}{\Sigma_e}\left[\Sigma_\theta - 0.5\left(\Sigma_r + \Sigma_z\right)\right], \tag{47}$$

$$\dot{\varepsilon}_z = \frac{\dot{\varepsilon}_e}{\Sigma_e}\left[\Sigma_z - 0.5\left(\Sigma_\theta + \Sigma_r\right)\right]. \tag{48}$$

For plane strain condition the axial strain rate disappears, i.e. $\dot{\varepsilon}_z = 0$.

$$\Sigma_z = 0.5\left(\Sigma_\theta + \Sigma_r\right). \tag{49}$$

Substituting Eq. (49) into the first two of Eqs. (47)-(48) the radial and circumferential strain rates are found to be

$$\dot{\varepsilon}_r = \frac{3\dot{\varepsilon}_e}{4\Sigma_e}\left(\Sigma_r - \Sigma_\theta\right), \tag{50}$$

$$\dot{\varepsilon}_\theta = \frac{3\dot{\varepsilon}_e}{4\Sigma_e}\left(\Sigma_\theta - \Sigma_r\right). \tag{51}$$

The Norton's creep constitutive model for FGPM is considered to be (Norton, 1929)

$$\dot{\varepsilon}_e = B t^n \Sigma_e{}^m, \tag{52}$$

where

$$B = 0.11\times10^{-21},\ \ m = 5,\ \ 0.33 < n < 0.50. \tag{53}$$

In this case the Von Mises equivalent stress is reduced to

$$\Sigma_e = \frac{1}{\sqrt{2}}\sqrt{\left(\Sigma_\theta - \Sigma_r\right)^2 + \left(\Sigma_\theta - \Sigma_z\right)^2 + \left(\Sigma_z - \Sigma_r\right)^2} = \frac{\sqrt{3}}{2}\left(\Sigma_\theta - \Sigma_r\right). \tag{54}$$

To obtain history of stresses, deformation and electric potential a numerical procedure based on the method of successive approximation has been tailored.

5. Numerical procedure to obtain history of stresses, deformation and electric potential

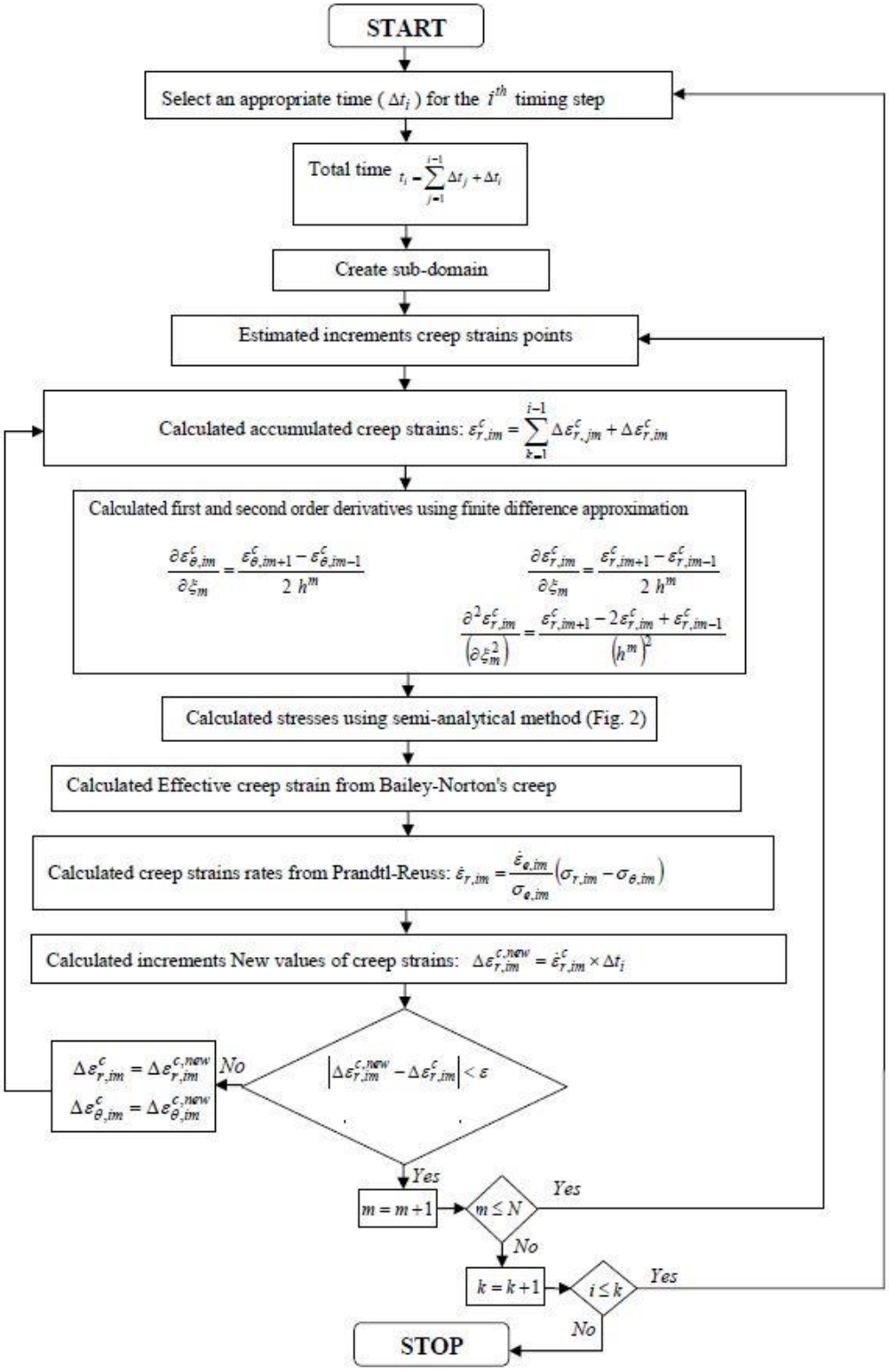
START
Select an appropriate time (Δt_i) for the i^{th} timing step
Total time $t_i = \sum_{j=1}^{i-1} \Delta t_j + \Delta t_i$
Create sub-domain
Estimated increments creep strains points
Calculated accumulated creep strains: $\varepsilon_{r,im}^{c} = \sum_{k=1}^{i-1} \Delta\varepsilon_{r,jm}^{c} + \Delta\varepsilon_{r,im}^{c}$
Calculated first and second order derivatives using finite difference approximation
$\frac{\partial\varepsilon_{\theta,im}^{c}}{\partial\xi_m} = \frac{\varepsilon_{\theta,im+1}^{c} - \varepsilon_{\theta,im-1}^{c}}{2\,h^m}$
$\frac{\partial\varepsilon_{r,im}^{c}}{\partial\xi_m} = \frac{\varepsilon_{r,im+1}^{c} - \varepsilon_{r,im-1}^{c}}{2\,h^m}$
$\frac{\partial^2\varepsilon_{r,im}^{c}}{\left(\partial\xi_m^2\right)} = \frac{\varepsilon_{r,im+1}^{c} - 2\varepsilon_{r,im}^{c} + \varepsilon_{r,im-1}^{c}}{\left(h^m\right)^2}$
Calculated stresses using semi-analytical method (Fig. 2)
Calculated Effective creep strain from Bailey-Norton's creep
Calculated creep strains rates from Prandtl-Reuss: $\dot{\varepsilon}_{r,im} = \frac{\dot{\varepsilon}_{e,im}}{\sigma_{e,im}}\left(\sigma_{r,im} - \sigma_{\theta,im}\right)$
Calculated increments New values of creep strains: $\Delta\varepsilon_{r,im}^{c,new} = \dot{\varepsilon}_{r,im}^{c} \times \Delta t_i$
$\left|\Delta\varepsilon_{r,im}^{c,new} - \Delta\varepsilon_{r,im}^{c}\right| < \varepsilon$
No
$\Delta\varepsilon_{r,im}^{c} = \Delta\varepsilon_{r,im}^{c,new}$
$\Delta\varepsilon_{\theta,im}^{c} = \Delta\varepsilon_{\theta,im}^{c,new}$
Yes
$m = m+1$
$m \le N$
Yes
No
$k = k+1$
$i \le k$
Yes
No
STOP

We have employed Mendelson's method of successive elastic solution to obtain history of stresses, displacement and electric potential as follows:

It was shown that creep strains and their derivatives are involved in non-homogenous part of differential Eq. (37) P_4. Immediately after loading the creep strains are zero and the solution is an elasticity problem. To solve differential Eq. (37) for long time after loading, method of successive elastic solution is used. Step by step procedure is explained in the algorithm as follows

6. Numerical results and discussion

The numerical results presented here are based on the material properties defined in Table 1 for PZT_5 (Jaffe and Berlincourt 1965). The temperature at the inner and outer surfaces of the FGPM cylinder are considered to be T_a=50℃ and T_b=25℃ respectively and the aspect ratio is χ=2. In this section, history of stresses, electric potential and radial displacement of the FGPM hollow cylinder for two cases of mechanical and electrical boundary conditions (Eqs. (44)-(45)) is investigated.

Figs. 3(a)-3(b) show radial stress history against dimensionless radius for mechanical and electrical boundary conditions, respectively. As can be seen, throughout the cylinder thickness, the

Table 1 Mechanical and electrical properties for PZT_5

property	PZT_5
c_{11}	111 (GPa)
c_{12}	75.2 (GPa)
c_{22}	120 (GPa)
e_{11}	15.78 (C/m^2)
e_{12}	−5.35 (C/m^2)
$\in_{11}$	7.4e−9 (C^2/Nm^2)
α_{r0}	8.53e−6 (1/K)
$\alpha_{\theta 0}$	1.99e−6 (1/K)
β_1	−2.5e−5 (c/m^{2}k)
ρ	7750 (kg/m^3)

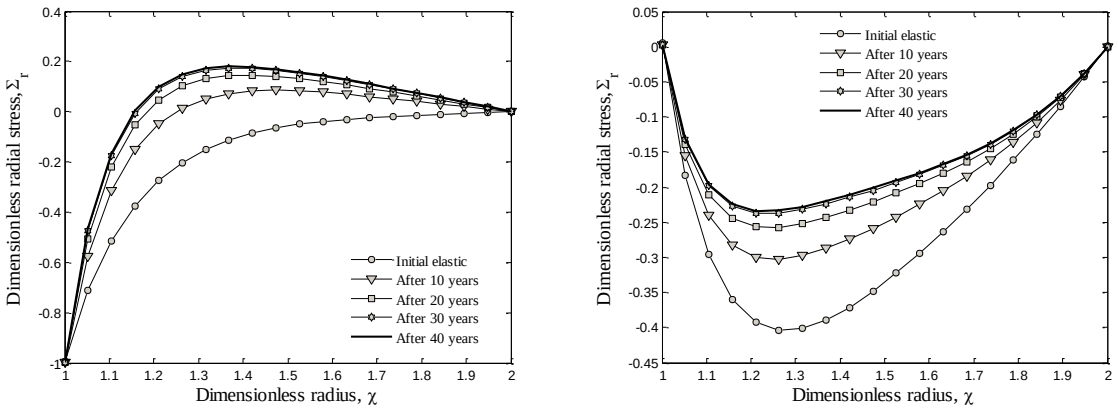

Fig. 3 History of radial stress for the FGPM cylinder for (a) mechanical boundary condition (b) electrical boundary condition

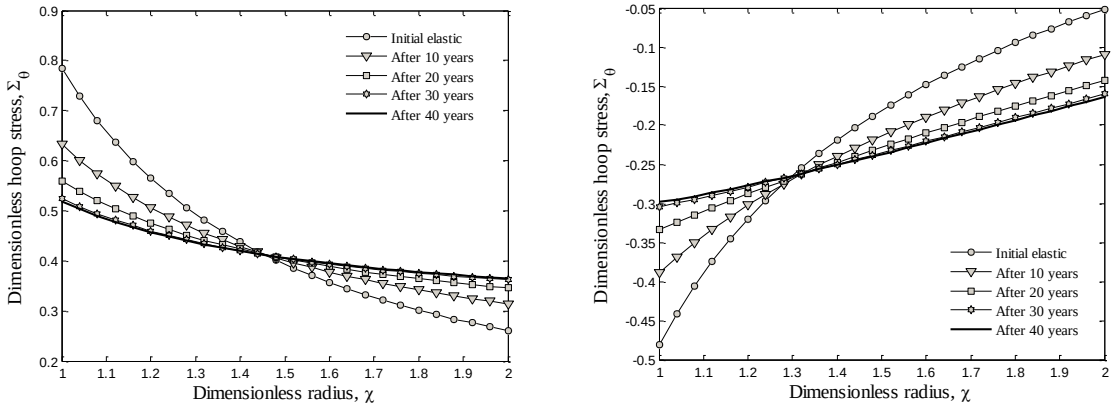

Fig. 4 History of circumferential stress for the FGPM cylinder for (a) mechanical boundary condition (b) electrical boundary condition

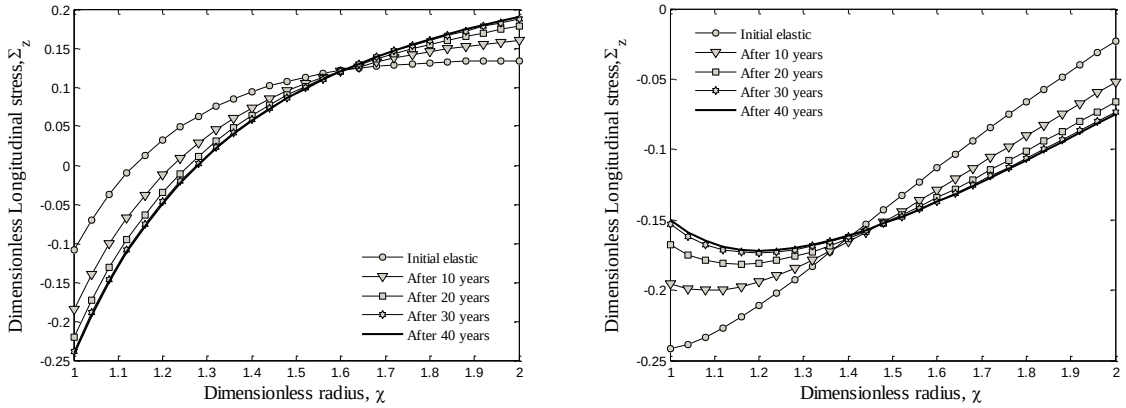

Fig. 5 History of longitudinal stress for the FGPM cylinder for (a) mechanical boundary condition (b) electrical boundary condition

absolute value of radial stress decreases with time. Maximum change in Σ_r occurs in the mid range of χ. The change in the rate of radial stress become less significant after 20, begin to converge after 30, and reaches steady state after 40 years. As can be seen from Figs. 3(a) and 3(b), radial stresses are constant with respect to time at the interior and exterior surfaces of the FGPM cylinder, satisfying the constant mechanical and electrical boundary conditions set out originally in Eqs. (44)-(45).

Figs. 4-5 demonstrate the plots of circumferential and longitudinal stresses across the cylinder thickness for mechanical and electrical boundary conditions, respectively. As can be seen from Fig. 4(a), the circumferential stress is positive for mechanical boundary condition, i.e., it remains tensile throughout the thickness. As far as the effect of time on these stresses is concerned, they decrease with time at the interior surface and increase with time at the exterior. Also, the same as the radial stresses, without commenting on the magnitude, the change in the rate of these stresses become less significant after 20, begin to converge after 30, and reaches steady state after 40 years. Reference stresses are also identified for circumferential and longitudinal stresses which are

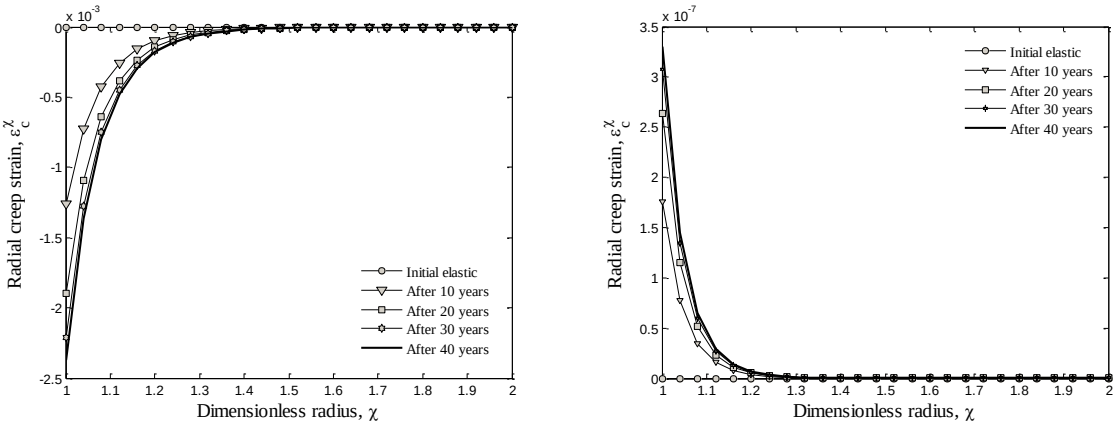

Fig. 8 History of radial creep strain for the FGPM cylinder for (a) mechanical boundary condition (b) electrical boundary condition

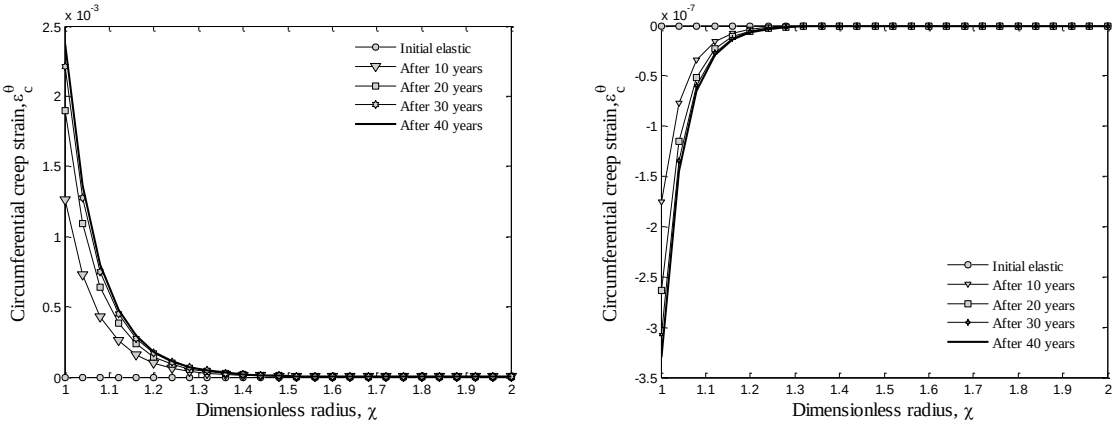

Fig. 9 History of circumferential creep strain for the FGPM cylinder for (a) mechanical boundary condition (b) electrical boundary condition

independent of time. Comparing stresses with and without the effect of electric potential one can find that imposing an electric potential significantly decreases the highly tensile circumferential stresses of the FGPM cylinder.

Despite different (but satisfied) boundary conditions at the inner and outer surfaces (see Eq. 45), the histories of the imposed through-thickness electric potentials as shown in Figs. 6(a)-6(b) for mechanical and electrical boundary conditions, respectively, is fairly similar to that of the compressive radial stress as far as the rate change is concerned. That is perhaps because the electric potential histories are induced by the compressive radial stress histories during creep deformation of the cylinder. This is expected from the piezoelectric characteristic point of view.

History of radial displacements is shown in Figs. 7(a)-7(b) for mechanical and electrical boundary conditions, respectively. It is clear that radial displacements increase with time at a decreasing rate during creep process of the cylinder and finally reaches a steady state at 40 years. Furthermore, maximum radial displacements occur at the interior surface and it decreases

smoothly towards the exterior.

As for the histories of radial and circumferential creep strains for mechanical and electrical boundary conditions, respectively, these are presented in Figs. (8)-(9). The radial and tangential strains are equal in magnitude but opposite in nature (sign) due to incompressibility condition ($\dot{\varepsilon}_r + \dot{\varepsilon}_\theta + \dot{\varepsilon}_z = 0$) and the assumption of plain strain condition ($\dot{\varepsilon}_z = 0$). The absolute value of both creep strains with time is much higher at the interior surface as compared with the exterior. As far as, the rate of change is concerned, this seems to increases to a maximum between 5 and 10 years, and then decreases until it reaches steady state around 30 years of operation.

7. Conclusions

Time-dependent creep analysis has been carried out to improve the performance and reliability of piezoactuators used for high-precision applications, when these devices are used even at room temperatures. Time-dependent thermo-electro-mechanical creep behavior of radially polarized FGPM hollow cylinder is investigated using an using a semi-analytical numerical method. History of stresses, electric potentials and displacements of two different combinations of mechanical and electrical boundary conditions are studied. The results show that in general a major redistribution for electric potential takes place throughout the thickness. Electric potentials are increasing with time in the same direction as the compressive radial stress histories. In fact the electric potential histories are induced by the compressive radial stress histories during creep deformation of the FGPM cylinder. It has also been concluded that imposing an electric potential significantly decreases the highly tensile tangential stresses.

References

Altenbach, H., Gorash, Y. and Naumenko, K. (2008), "Steady-state creep of a pressurized thick cylinder in both the linear and the power law ranges", *Acta Mech.*, **195**, 263-274.

Bahtui, A. and Eslami, M.R. (2007), "Coupled thermoelasticity of functionally graded cylindrical shells", *Mech. Res. Comm.*, **34**, 1-18.

Bayat, M., Saleem, M., Sahari, B.B., Hamouda, A.M.S. and Mahdi, E. (2009), "Mechanical and thermal stresses in a functionally graded rotating disk with variable thickness due to radially symmetry loads", *Int. J. Press. Vess. Pip.*, **86**, 357-372.

Bhatnagar, N.S. and Arya, V.K. (1974), "Large strain creep analysis of thick-walled cylinders", *Int. J. Non-Linear Mech.*, **9**, 127-40.

Dai, H.L., Fu, Y.M. and Dong, Z.M. (2006), "Exact solutions for functionally graded pressure vessels in a uniform magnetic field", *Int. J. Solid. Struct.*, **43**, 5570-5580.

Dai, H.L., Jiang, H.J. and Yang, L. (2012), "Time-dependent behaviors of a FGPM hollow sphere under the coupling of multi-fields", *Solid State Sci.*, **14**, 587-597.

Ghorbanpour Arani, A., Kolahchi, R. and Mosallaei Barzoki, A.A. (2011), "Effect of material in-homogeneity on electro-thermo-mechanical behaviors of functionally graded piezoelectric rotating shaft", *Appl. Math. Model.*, **35**, 2771-2789.

Ghorbanpour Arani, A., Kolahchi, R., Mosallaie Barzoki, A.A. and Loghman, A. (2011), "Electro-thermo-mechanical behaviors of FGPM spheres using analytical method and ANSYS software", *Appl. Math. Model.*, **36**, 139-157.

Ghorbanpour Arani, A., Mosallaie Barzoki, A.A., Kolahchi, R., Mozdianfard, M.R. and Loghman, A.

(2011c), "Semi-analytical solution of time-dependent electro-thermo-mechanical creep for radially polarized piezoelectric cylinder", *Compos. Struct.*, **89**, 1494-1502.
Jabbari, M., Sohrabpour, S. and Eslamic, M.R. (2002), "Mechanical and thermal stresses in a functionally graded hollow cylinder due to radially symmetric loads", *Int. J. Press. Vess. Pip.*, **79**, 493-497.
Jaffe, H. and Berlincourt, D.A. (1965), "Piezoelectric transducer materials", *Proc. IEEE*, **53**, 1372-1386.
Kordkheili, S.A.H. and Naghdabadi, R. (2007), "Thermoelastic analysis of a functionally graded rotating disk", *Compos. Struct.*, **79**, 508-516.
Liew, K.M., Kitipornchai, S., Zhang, X.Z. and Lim, C.W. (2003), "Analysis of the thermal stress behaviour of functionally graded hollow circular cylinders", *Int. J. Solid. Struct.*, **40**, 2355-2380.
Loghman, A., Ghorbanpour Arani, A., Amir, S. and Vajedi, A. (2010), "Magnetothermoelastic creep analysis of functionally graded cylinders", *Int. J. Press. Vess. Pip.*, **87**, 389-395.
Pai, D.H. (1967), "steady-state creep analysis of thick-walled orthotropic cylinders", *Int. J. Mech. Sci.*, **9**, 335-482.
Loghman, A., Aleayoub, S.M.A. and Hasani Sadi, M. (2012), "Time-dependent magnetothermoelastic creep modeling of FGM spheres using method of successive elastic solution", *Appl. Math. Model.*, **36**, 836-845.
Norton, F.H. (1929), *The creep of steel at high temperatures*, McGraw-Hill, London.
Penny, R.K. and Marriott, D.L. (1995), *Design for creep*, CHAPMAN & HALL, London.
Sim, R.G. and Penny, R.K. (1971), "Plane strain creep behaviour of thick-walled cylinders", *Int. J. Mech. Sci.*, **13**, 987-1009.
Simonian, A.M. (1979), "Calculation of thermal stresses in thick-walled cylinders taking account of non-linear creep", *Int. J. Eng. Sci.*, **17**, 513–522.
Tiersten, H.F. (1969), *Linear piezoelectric plate vibrations*, Plenum Press, New York.
Yang, Y.Y. (2000), "Time-dependent stress analysis in functionally graded materials", *Int. J. Solid. Struct.*, **37**, 7593-7608.
You, L.H., Zhang, J.J. and You, X.Y. (2005), "Elastic analysis of internally pressurized thick-walled spherical pressure vessels of functionally graded materials", *Int. J. Press. Vess. Pip.*, **82**, 347-354.
Zhou, D. and Kamlah, M. (2006), "Room-temperature creep of soft PZT under static electrical and compressive stress loading", *Acta Mater.*, **54**, 1389-1396.

CC